Finite Element Modeling and Experimental Validation of Microstructural Changes and Hardness Variation During Gas Metal Arc Welding of Aisi 441 Ferritic Stainless Steel

SERAFINO CARUSO (serafino.caruso@unical.it)
University of Calabria: Universita della Calabria https://orcid.org/0000-0003-4090-6133
STANO IMBROGNO
University of Birmingham

Research Article

Keywords: Gas metal arc welding, Grain size, AISI 441, Finite element modeling, Hardness, Heat source model, Heat affected zone

Posted Date: September 21st, 2021

DOI: https://doi.org/10.21203/rs.3.rs-909068/v1

FINITE ELEMENT MODELING AND EXPERIMENTAL VALIDATION OF MICROSTRUCTURAL CHANGES AND HARDNESS VARIATION DURING GAS METAL ARC WELDING OF AISI 441 FERRITIC STAINLESS STEEL

Serafino Caruso[1*], Stano Imbrogno[2]

[1] Department of Mechanical, Energy and Management Engineering, University of Calabria, Rende, CS 87036, Italy. ORCID: 0000-0003-4090-6133

[2] School of Metallurgy and Materials, University of Birmingham, Birmingham B15 2TT, UK. ORCID: 0000-0002-9988-9860

Corresponding author.

E-mail address: serafino.caruso@unical.it (S. Caruso)

ABSTRACT

Grain growth and hardness variation occurring in high temperature Heat Affected Zone (HAZ) during the welding processes are two thermal dependant aspects of great interest for both academic and industrial research activities. This paper presents an innovative Finite Element (FE) model capable to describe the grain growth and the hardness decrease that occur during the Gas Metal Arc Welding (GMAW) of commercial AISI 441 steel. The commercial FE software SFTC DEFORM-3D^{TM} was used to simulate the GMAW process and a user subroutine was developed including a physical based model and the Hall-Petch (H-P) equation to predict grain size variation and hardness change. The model was validated by comparison with the experimental results showing its reliability in predicting important welding characteristics temperature dependant. The study provides an accurate numerical model (i.e. user subroutine, heat source fitting, geometry,...) able to successfully predict the thermal phenomena (i.e. coarsening of the grains and hardening decrease) that occur in the HAZ during welding process of ferritic stainless steel.

Keywords: Gas metal arc welding, Grain size, AISI 441, Finite element modeling, Hardness, Heat source model, Heat affected zone.

NOMENCLATURE

C_0	numerical constant
C_1	numerical constant
D	current grain size
D_0	initial grain size
FE	finite element
FEM	finite element method
FZ	fusion zone
GMAW	gas metal arc welding
GTAW	gas tungsten arc welding
HAZ	heat affected zone
H-P	Hall-Petch
HV	hardness Vickers
IRC	infra-red camera
Q	activation energy for grain growth
R	gas constant
T	current temperature
TIG	tungsten inert gas
a	heat source parameter
b	heat source parameter
c_1	heat source parameter
c_2	heat source parameter
d	average grain size
k	numerical constant
k_y	numerical constant
k_0	numerical constant
σ_y	yield strength
σ_0	numerical constant
m	numerical constant
t	time

INTRODUCTION

The welding process is one of the most important material joining method among the various manufacturing processes. Although its simplicity of execution, usually involving the deposition of molten filler metal and the localized heat input, the weld region close to the welded joint experiences complex thermo-mechanical cycles due to localized heating and cooling steps. Generally, these result in non-uniform expansion (heating phase) and shrinking (cooling phase) sequence of the region between the base metal and the welded material leading to distortion [1-4] particularly detrimental for the functional performance and service safety of the component.

For this reason, an accurate knowledge of the thermo-mechanical aspects featuring the joining procedure and its evolution during the process execution is required with the aim to identify, control and minimize problems to achieve the desired and reliable outputs. Besides, considering the important role of the FE modeling as predictive tool, the research focused on welding process made significant efforts both in the experimental and numerical fields investigating several aspects of the joining process: distortion, residual stresses [5, 6], clamping system [7, 8], temperature fields, heat source modelling [9, 10]. J.J. Xu et al. [11] carried out an uncoupled 3D thermal and mechanical analysis by SYSWELD, a commercial software code for welding simulations, to predict and analyse temperature and residual stress during a single weld bead deposition on AISI 316L austenitic steel by Tungsten Inert Gas (TIG) welding. The heat source was modelled through the heat source fitting tool considering a double ellipsoid heat source model and the measured welding temperatures. Subsequently, the authors validated the developed numerical model comparing the simulated bead boundaries profiles, temperature fields and predicted residual stresses with the experimental outcomes. Moreover, they observed that the influence of the clamping restraint on the residual stresses profile was not so significant. S. T. Prabakaran et al. [12] investigated the mechanical and metallurgical effects of TIG welding of INCONEL 718 plates by an experimentally validated numerical model. A deep analysis of the thermal stress distribution, the HAZ size and the hot cracking

susceptibility of the weld joint was carried out using Finite Element Method (FEM) solution. K. R. Balasubramanian et al. [13] developed a FEM to simulate the laser beam welding of AISI 304 stainless steel sheet. The experimental campaign of about 81 tests, varying the beam power, the welding speed, the beam angle and the gas flow rate, was carried out to validate a robust numerical model able to simulate the bead profile. M. Zubairuddin et al. [14] analysed the residual stress and distortion occurring in a modified 9Cr-1Mo steel plates when conducting gas tungsten arc welding (GTAW). The authors developed a 3D FEM able to predict accurately the residual stress profile across the fusion zone (FZ), the thermal cycles and the component distortion. The comparison between numerical and experimental results confirmed the better accuracy of the large distortion theory in welding thin plates. S. K. Panda et al. [15] proposed a numerical model to predict the formability of DP980 steel sheets when performing laser welding. The authors found that both the strength and the ductility of laser welded blanks decreased due to the softened outer-HAZ: the higher the softened HAZ the lower the strength of the material. A. A. Deshpande et al. [16] showed a FE modelling of heat source and distortion in TIG-welded butt joint of SS304 sheets. The FE model was firstly validated by comparison with experimental macrographs of the weld bead, the thermal cycle and the residual distortion. Subsequently, the authors used the model to investigate the effects of natural and forced convection, of the constraint release time and of the welding path sequence. R. Konar et al. [17] studied the residual stresses of dissimilar weld joint of austenitic X5CrNi18-10 and ferritic S355J2H steel by numerical simulation. The FE analysis of the weld joint also proved to be a valid tool for thermal and hardness prediction. V. V. Narayanareddy et al. [18] developed a FEM of the TIG welding during joining 316L stainless steel. After modelled and validated the heat source based on Goldak's shape, the authors investigated the influence of welding process parameters (i.e. current, voltage and weld speed) on the heat energy input. A significant effect of the process parameters on the peak temperature on FZ and HAZ extension and shape was also observed. Coz et al. [19] compared the type of distortion and the magnitude induced by TIG welding on austenitic and duplex stainless steels through the FE simulation. The authors showed that the material properties affected the final deformed shape.

The literature analysis showed that the microstructural alteration within the HAZ has significant effects on the final properties of the part. For this reason, it is useful to develop an adequate FE numerical model able to predict and control the thermo-mechanical phenomena that occur during the investigated process since they are fundamental for the mechanical performances and the quality of the final product.

This work wants to scientifically contribute to deliver a novel numerical model that takes into account the grain size evolution to predict the microstructural changes and the hardness variation in the HAZ during GMAW of AISI 441 ferritic stainless steel. The innovative aspect of this work is represented by the use of the commercial FE software SFTC DEFORM-3D^{TM}, designed to analyse metal forming, heat treatment, machining and mechanical joining processes. A customized user sub-routine that allows the numerical model to predict the grain growth and hardness variation during the investigated process was developed and implemented in the commercial FE software. Moreover, the numerical procedure for the heat source definition: geometry and movement is also reported. Finally, a comparison between the numerical results and the corresponding experimental data was carried out to validate the model. The effectiveness of the proposed numerical tool to measure and control the grain size evolution

and the related hardness variation, characterizing the HAZ is shown. It is important to highlight that the present work represents a first attempt to simulate the welding process by using DEFORM 3D FE code developed to analyse other types of processes.

Table 1 AISI 441-Material chemical composition (weight %)

Elements	Cr	C	Mn	Si	Al	Ti	Nb	Mo	Fe
Weight %	17.83	0.01	0.24	0.60	0.006	0.13	0.55	0.01	Balance

Table 2 AISI 307-Material chemical composition (weight %)

Elements	Cr	C	Mn	Si	P	S	Ni	Mo	Fe
Weight %	20.30	0.08	3.3	0.90	0.04	0.015	8.50	1.5	Balance

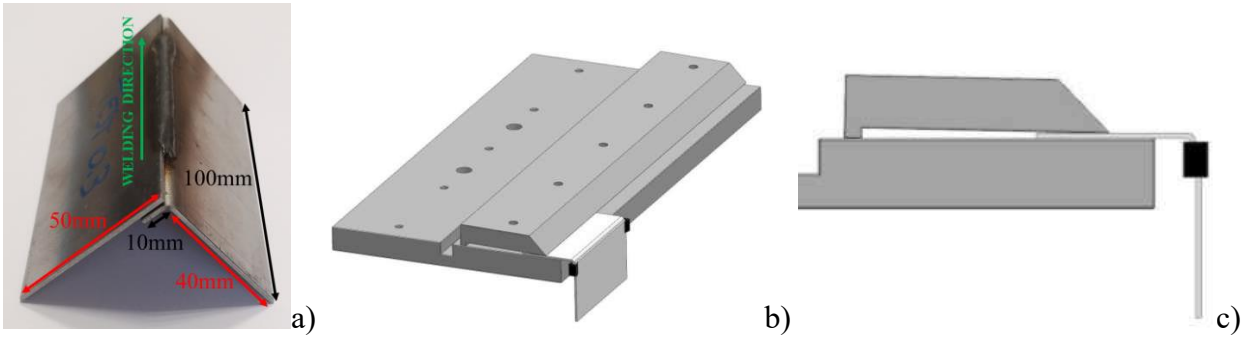

a) b) c)

Fig. 1 Sample geometry a), clamping setup b) and c)

EXPERIMENTAL PROCEDURE

GMAW experiments were performed on AISI 441 ferritic stainless steel (Table 1) by a fully automated torch movement. The welds were conducted on two plates (248$HV_{0.01}$ and 1.5mm thick) and the geometry and the clamping setup are reported in Fig. 1. Furthermore, three parts were welded to statistically assess the process. The welding process parameters were 220A current, 11.9V voltage, 13.33mm/sec weld speed and 12.2mm/min filler material speed deposition (AISI 307 with a diameter of ϕ=1mm, Table 2). Pure Argon with a flow rate of 15L/min was used as shielding gas. After welding, a sample of 30mm length (welding direction, Fig. 1a) was cut, and the cross section was mounted with cold resin for the metallographic analysis and hardness measurement. The metallographic preparation consisted of mechanical polishing and then etching with the Keller's reagent (92ml of distilled water, 6ml of nitric acid, 2ml of hydrochloric acid, 2ml hydrofluoric acid). The cross section was analysed by an optical microscope to characterise the weld bead geometry, the HAZ extension and the grain size evolution measurements. Fig. 2 reports the micrograph obtained by the optical microscope: the weld metal (melted part), the HAZ and the base metal (unaffected material) are clearly distinguishable. The HAZ size was found approximately equal to 450±50µm. The measurement was determined by measuring and comparing both the grain size evolution and the hardness change. The micro-hardness ($HV_{0.01}$) was investigated by an instrumented micro-nano indenter.

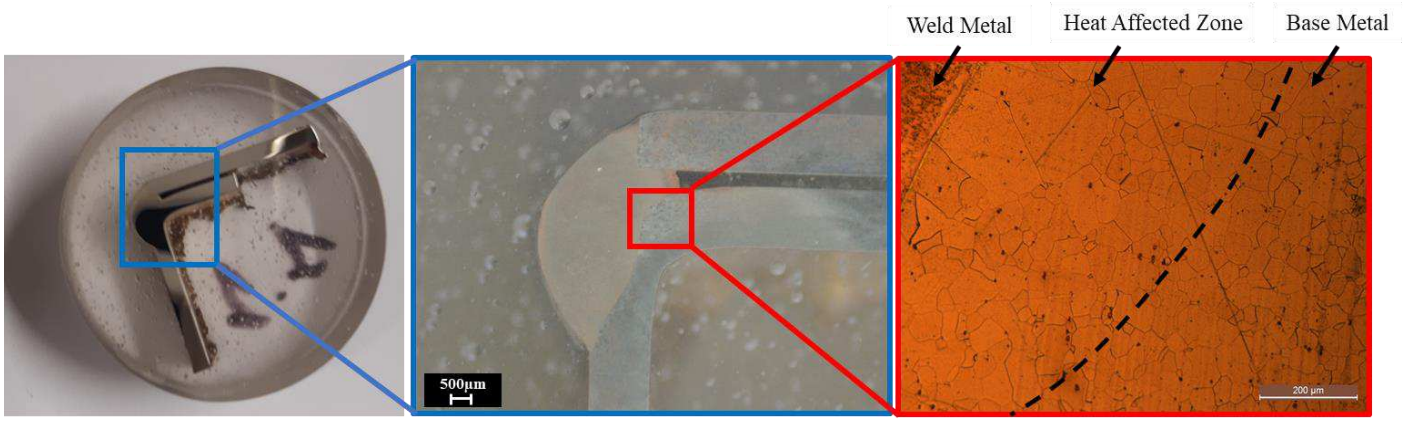

Fig. 2 Transverse section metallographic analysis

Fig. 3 shows the grain size evolution along the different zones obtained by welding process. In particular, Fig. 3a reports the grain size of the unaffected zone, representing the base material with an average value of 35µm. Fig. 3b shows the grains of the HAZ that are coarser (72µm) than the ones reported in Fig. 3a due to the temperature increase that triggered the grain growth. Fig. 3c represents the grains of the weld metal with an average value of 10µm. Despite the size difference, the grain maintained an equiaxial shape in all the investigated zones.

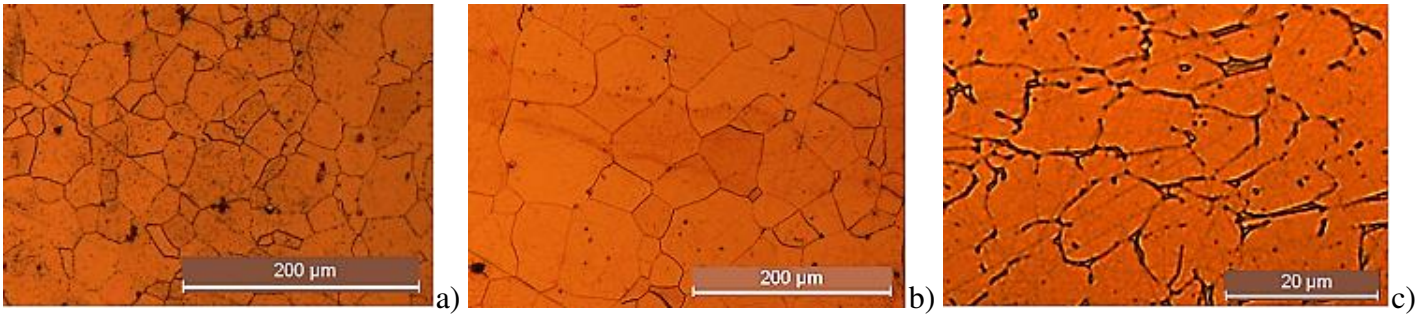

a) b) c)

Fig. 3 Transverse section grain size a) base metal, b) HAZ and c) weld metal

The micro-hardness was measured considering an indentation matrix (22x3 points) as reported in Fig. 4a. As reported in Fig. 4b, the hardness significantly decreased from the base metal (248HV) to the HAZ (215HV) with a reduction of 33HV (-13%). On the other hand, a hardness value of 295HV was measured on the weld metal, with a significant increase of 80HV (+37%) when compared with the HAZ, and of 47HV (+19%) when compared with the base metal. Therefore, the thermal phenomena effects on the HAZ softening with a consequent material strength reduction due to both hardness decrease and grain growth are quite evident. Indeed, the material strengthening is an inverse function of the square root of the grain size: the coarser the grain size, the lower is the strength according to Hall-Petch effect (Equation 1)

$$\sigma_y = \sigma_0 + \frac{k_y}{\sqrt{d}} \quad (1)$$

Where σ_y is the yield strength, k_y is the strengthening coefficient, σ_0 is a material constant and d is the average grain size.

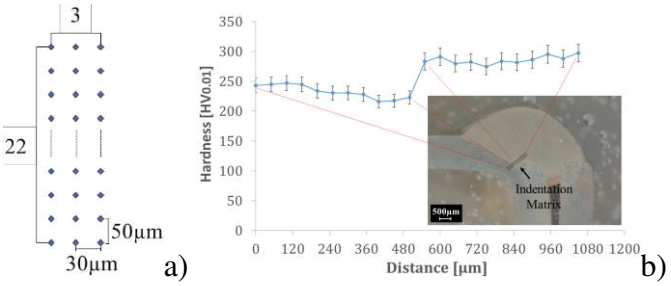

Fig. 4 a) Hardness indentation matrix and b) transverse section indentation measurement

The thermal field was acquired by a FLIR A655sc Infra-Red Camera (IRC), therefore the temperature profiles of the welded surfaces of the specimens were evaluated. A range temperature acquisition of 100-650°C was set, leading to analyse the cooling step of the process that, for its duration, is considered the main reason for the distortion. The thermal analysis allowed to evaluate the cooling temperature-trend focusing on three points located at the beginning, the centre and the end of the weld bead, respectively as shown in Fig. 5.

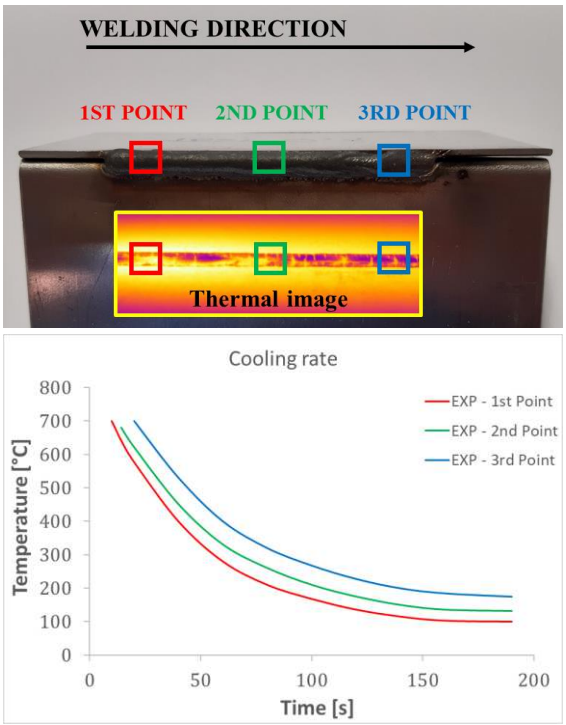

Fig. 5 Cooling temperature trend

The temperature profiles reported in Fig. 5 were used to calibrate the model by an iterative trial and error procedure. Moreover, the same approach was used to evaluate the temperature and the convection coefficient of the heat exchange windows implemented in DEFORM to model the welding heat source.

NUMERICAL MODEL

The commercial FE software SFTC DEFORM-3D™ was used for modeling the GMAW process of the commercial AISI 441 ferritic stainless steel. The two plates were modelled as a plastic body meshed with 50000 iso-parametric tetrahedral elements, while for the weld bead a plastic model with 32000 elements was considered (Fig. 6).

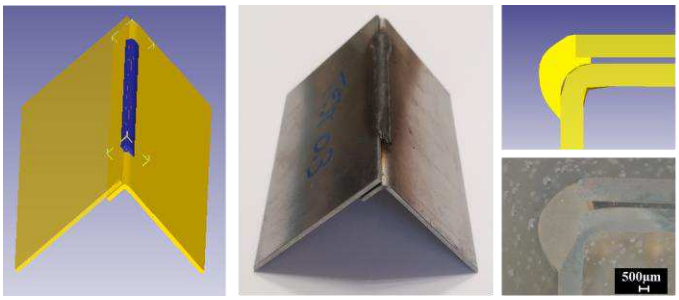

Fig. 6 Finite element modeling

To simulate the GMAW a three-dimensional Goldak's double-ellipsoid heat source model was considered, where a, b, c_1 and c_2 (Fig. 7a) are the ellipsoidal heat source parameters, respectively the half width, the depth of penetration, the front length of molten pool and the rear length of molten pool, respectively.

The above cited heat source model was implemented in DEFORM defining a series of 3D heat exchange windows reproducing the shape of the Goldak's double-ellipsoid (Fig. 7b) and characterized by a movement velocity of 13.33mm/sec according to the experimental welding speed process parameter.

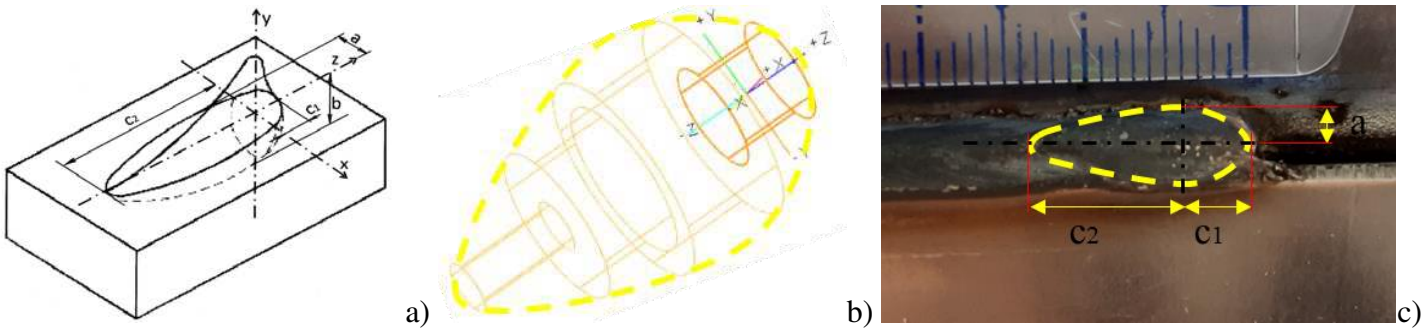

Fig. 7 a) Goldak's double-ellipsoid heat source model, b) DEFORM heat exchange windows for heat source modeling and c) measurements of the ellipsoidal heat source parameters a, c_1 and c_2

All the above cited heat source parameters, the temperature and the convection coefficient of the heat exchange windows were experimentally determined considering the weld bead geometry, the HAZ size and the cooling temperature trend. In detail, the parameters a, c_1 and c_2 were measured on the welded component (Fig. 7c), while the parameter b, the temperature and the convection coefficient of the heat exchange windows were calibrated by an iterative trial and error procedure of comparison between the numerical and experimental HAZ size and the cooling profile (Fig. 8).

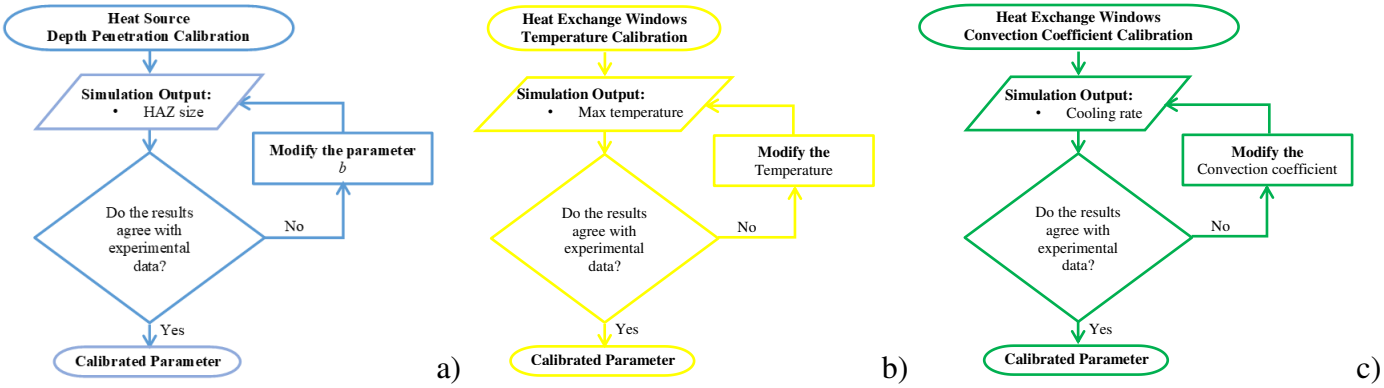

Fig. 8 Iterative procedure to calibrate a) the heat source depth penetration, b) the temperature of the heat exchange window and c) the convection coefficient of the heat exchange window

The thermal phenomena affecting the microstructure (i.e. grain size) of the HAZ was predicted by implementing a customized user subroutine involving the classic kinetic theory for grain growth [20, 21], Equation 1.

$$D^m - D_0^m = t \cdot k \tag{1}$$

Where D is the current grain size, D_0 is the initial grain size, m is the grain growth exponent, k is the kinetic constant and t is the soaking time. The grain growth kinetic constant k can be expressed by Arrhenius form as function of the temperature, Equation 2.

$$k = k_0 exp\left(-\frac{Q}{RT}\right) \tag{2}$$

Where k_0 is a pre-exponential constant, Q is the activation energy for grain growth, R is the gas constant and T is the temperature. Using Equation 2 in Equation 1 it is possible to define the expression for the grain growth kinetics, Equation 3.

$$D = \sqrt[m]{tk_0 exp\left(-\frac{Q}{RT}\right) + D_0^m} \quad (3)$$

All the values of Equation 3 are listed in Table 3.

Table 3 Numerical parameters for the grain growth kinetics

Q [J/mol]	**R [J/mol*K]**	**m**	**D_0 [mm]**
240000	8.314	4	0.035
[22]	[22]	[21]	Exp

For $t*k_0$ it was considered a constant value, validated during simulations and set equal to 10^5.

Finally, the hardness modification depending on the grain size evolution was calculated according to the H-P equation that considers hardness evolution as an inverse function of the grain size (Equation 4):

$$HV = C_0 + \frac{C_1}{\sqrt{d}} \quad (4)$$

Where C_0 and C_1 are two material constants while d represents the average grain size. The value of C_0 and C_1, were determined through the previously measured values of the material hardness and grain size of both HAZ and base metal and were set equal to 139.1 and 20.38, respectively.

FE VALIDATION AND RESULTS

The FE model was validated by comparing the experimental results of the cooling rate, grain size evolution and hardness variation with the corresponding numerical data.

Fig. 9a shows the uniform and stable numerical temperature profile while in Fig. 9b it is reported the comparison between the numerical HAZ with the experimental metallographic analysis.

The comparison analysis highlighted a small difference of about 50μm regarding the HAZ size prediction with a relative error of 15%. This acceptable difference between the numerical and the experimental data suggest that the developed numerical procedure is enough robust and confirms the correctness of the implemented numerical method in DEFORM 3D for the heat source shape modeling procedure. The reason of the difference between numerical and experimental outcomes could be due to i. the accuracy of the experimental data, ii. the calibration procedure implemented to define the numerical constants of the FE model and of the user subroutine and iii. the mesh discretization.

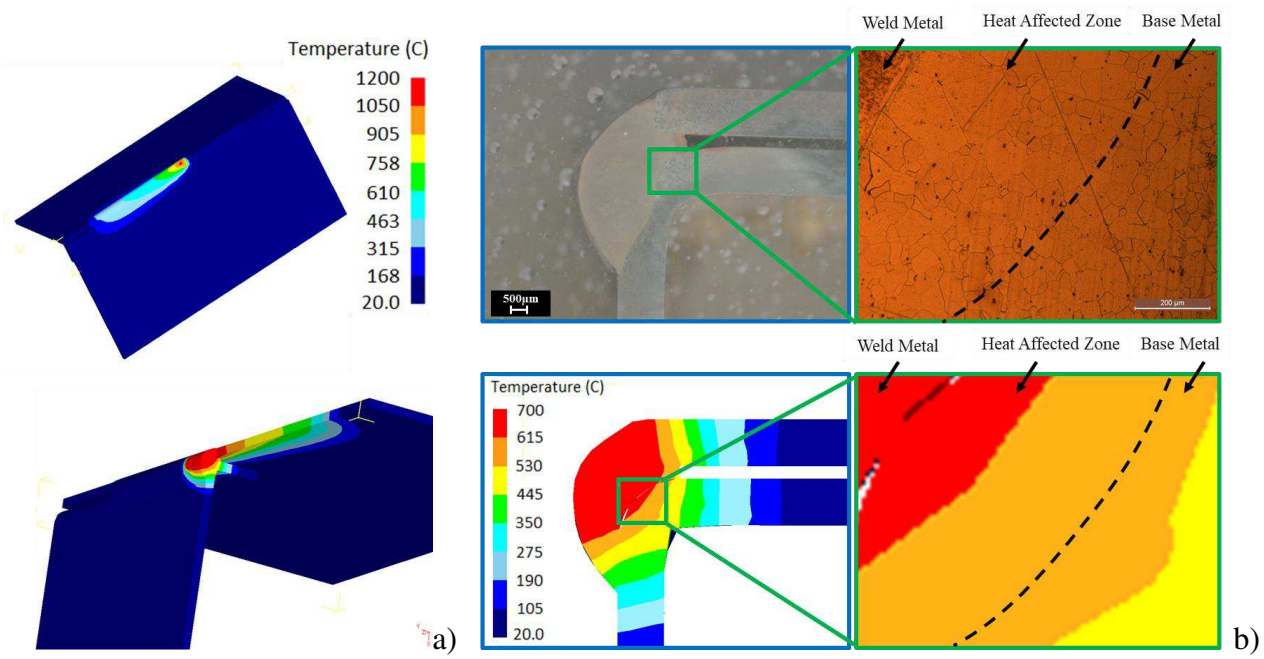

Fig. 9 a) Numerical temperature profile and b) validation of the predicted welding zones

Fig. 10 shows the prediction of the grains (region interested by the grain growth) and the hardness variation. These results higlight the reliability of the developed numerical model and the user subroutines to successfully predict the thermal phenomena that occur during GMAW process and the related metallurgical changes. In particular, due to the high reached temperature a new microstructure characterized by coarser grain size was computed and consequently this result affected the material hardness, as experimentally observed, resulting in a softer HAZaccording to Equation 4.

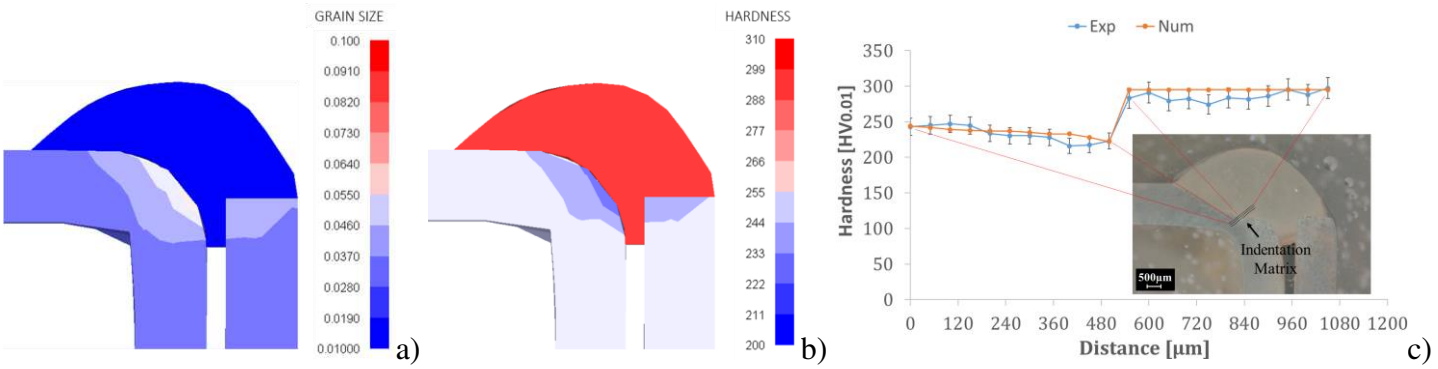

Fig. 10 Numerical predicted a) grain size [mm] and b) hardness [$HV_{0.01}$] and c) comparison between measured and predicted hardness variation c)

The numerical results, in agreement with those experimentally found, show that after the GMAW the evolution of the microstructure results in an average grain size increase that resulted quite coarser in the HAZ compared with the base metal. Thus, according to the inverse function of H-P equation (Equation 4), the hardness decreases showing that the thermal phenomena, characterizing the GMAW process,

cause severe microstructural and mechanical properties changes (Fig. 10).

DISCUSSION AND CONCLUSIONS

In this work a numerical model was developed to describe the grain size evolution and the hardness change within the HAZ during GMAW process of commercial AISI 441 ferritic stainless steel plates.

The commercial FE software SFTC DEFORM-3D^{TM} was used for the numerical analysis and a customized user subroutine was implemented for predicting the grain size and the hardness evolution according to the classic kinetic theory and the H-P relation respectively. The present work represents a first attempt to simulate the welding process by using a FE code developed to analyse other types of processes. In particular, the possibility to model the Goldak's double-ellipsoid heat source by a series of heat exchange windows tool available in the used software was validated. The good results obtained by the comparison of the predicted and the experimental HAZ size confirmed the effectiveness of developed model to properly include the heat source shape to predict the thermal fields. Moreover, the numerical results were validated by comparison with those experimentally found demonstrating the effectiveness of the customized model and the user subroutines to successfully predict the grain growth evolution and the hardness decrease within the HAZ due to the high temperatures induced by GMAW. Thus, the proposed FE strategy can be used to properly simulate the GMAW process of commercial AISI 441 ferritic stainless steel plates, allowing to consider the microstructural characteristics that affect the material performance. The developed numerical tool can be potentially employed during GMAW process to accurately monitor and control the desired microstructure, and consequently the mechanical performances, required to the welded products.

DECLARATIONS

Funding: Not applicable.

Conflicts of interest/Competing interests: The authors have no conflicts of interest to declare that are relevant to the content of this article.

Availability of data and material: Not applicable

Code availability: commercial FE software SFTC DEFORM-3D^{TM}

Authors' contributions: Conceptualization, S.C. and S.I.; methodology, S.C. and S.I. software, S.C.; validation, S.C.; formal analysis, S.I.; investigation, S.C. and S.I.; resources, S.C. and S.I.; data curation, S.C. and S.I.; writing—original draft preparation, S.C. and S.I.; writing—review and editing, S.C. and S.I.; visualization, S.I.; supervision, S.C. All authors have read and agreed to the published version of the manuscript.

Ethics approval: Not applicable.

Consent to partecipate: Not applicable

Consent for publication: Not applicable

REFERENCES

[1] Venkatkumar D, Ravindran D (2016) 3D finite element simulation of temperature distribution, residual stress and distortion on 304 stainless steel plates using GTA welding. J Mech Sci Technol 30: 67–76. https://doi.org/10.1007/s12206-015-1208-5.

[2] Balram Y, Vishu Vardhan T, Sridhar Babu B, Venkat Ramana G, Preethi C (2019) Thermal stress analysis of AISI 316 stainless steels weldments in TIG and pulse TIG welding processes. Mater Today: Proc 19(2): 182-187. https://doi.org/10.1016/j.matpr.2019.06.695.

[3] Vasantharaja P, Maduarimuthu V, Vasudevan M, Palanichamy P (2012) Assessment of residual stresses and distortion in stainless steel weld joints. Mater Manuf Process 27:1376–1381, https://doi.org/10.1080/10426914.2012.663135.

[4] Sule J, Ganguly S, Coules H, Pirling T (2015) Application of local mechanical tensioning and laser processing to refine microstructure and modify residual stress state of a multi-pass 304L austenitic steels welds. J Manuf Process Int J Plast 18: 141-150. https://doi.org/10.1016/j.jmapro.2015.03.003.

[5] Puliyaneth M, Chen H (2021) Study on the effect of welding residual stress on creep-cyclic plasticity behaviour. Int J Press Vessels Pip 193: 104444. https://doi.org/10.1016/j.ijpvp.2021.104444.

[6] Chuan L, Jianxun Z, Jing N (2009) Numerical and Experimental Analysis of Residual Stresses in Full-Penetration Laser Beam Welding of Ti6Al4V Alloy. Rare Metal Mat Eng 38(): 1317-1320. https://doi.org/10.1016/S1875-5372(10)60066-5.

[7] Ordieres J, Rodríguez E, Bayón A, Caixas J, Barbensi A, Martín C, (2021) Determination of the influence of clamping on welding distortion applied to PS2 mock-up using finite element simulations. Fusion Eng Des 166: 112327. https://doi.org/10.1016/j.fusengdes.2021.112327 .

[8] Woo D, Kitamura M, Takezawa A (2020) Systematic method for positioning clamps and strongbacks based on their influence on welding displacements. Ocean Eng 202: 107084. https://doi.org/10.1016/j.oceaneng.2020.107084.

[9] Mondal A K, Kumar B, Bag S, Nirsanametla Y, Biswas P (2021) Development of avocado shape heat source model for finite element based heat transfer analysis of high-velocity arc welding process. Int J Therm Sci 166: 107005. https://doi.org/10.1016/j.ijthermalsci.2021.107005.

[10] Unni A K, Vasudevan M (2021) Determination of heat source model for simulating full penetration laser welding of 316 LN stainless steel by computational fluid dynamics. Mater Today: proc 45(6): 4465-4471. https://doi.org/10.1016/j.matpr.2020.12.842.

[11] Xu J J, Gilles P, Duan Y G, Yu C (2012) Temperature and residual stress simulations of the NeT single-bead-on-plate specimen using SYSWELD. Int J Press Vessels Pip 99-100: 51-60. http://dx.doi.org/10.1016/j.ijpvp.2012.08.002.

[12] Prabakaran S T, Sakthivel P, Shanmugam M, Satish S, Muniyappan M, Shaisundaram V S (2021) Modelling and experimental validation of TIG welding of INCONEL 718. Mater Today: Proc 37(2): 1917-1931. https://doi.org/10.1016/j.matpr.2020.07.482.

[13] Balasubramanian K R, Suthakar T, Sankaranarayanasamy K (2012) Finite Element analysis of heat distribution in laser beam welding of AISI 304 Stainless Steel sheet. Int J Manuf 7(1): 42-58. DOI: 10.1504/IJMR.2012.045243.

[14] Zubairuddin M, Albert S K, Mahadevan S, Vasudevan M, Chaudhari V, Suri V K (2014) Experimental and finite element analysis of residual stress and distortion in GTA welding of modified 9Cr-1Mo steel. J Mech Sci Technol 28(12): 5095-5105. DOI 10.1007/s12206-014-1132-0.

[15] Panda S K, Sreenivasan N, Kuntz M L, Zhou Y (2008) Numerical Simulations and Experimental Results of Tensile Test Behavior of Laser Butt Welded DP980 Steels. J Eng Mater Technol 130(4): 041003. https://doi.org/10.1115/1.2969256.

[16] Deshpande A A, Xu L, Sun W, McCartney D G, Hyde T H (2011) Finite-element-based parametric study on welding-induced distortion of TIG-welded stainless steel 304 sheets. J Strain Anal Enf Des 46(4): 267-279. https://doi.org/10.1177/0309324711398763.

[17] Konar R, Patek M (2017) Numerical simulation of dissimilar weld joint in SYSWELD simulation software. Tech Gaz 24(1): 137-142. https://doi.org/10.17559/TV-20150513074103.

[18] Narayanareddy V V, Srinivasa R D, Krishnaveni M N V, Amareswarireddy M (2015) Finite Element Modeling of TIG Welding for 316L Stainless Steel Plate using Sysweld. Int J Eng Mang Res 5(2): 390-397. ISSN (ONLINE): 2250-0758, ISSN (PRINT): 2394-6962.

[19] Del Coz Díaz J J, Menéndez Rodríguez P, García Nieto P J, Castro-Fresno D (2010) Comparative analysis of TIG welding distortions between Austenitic and Duplex Stainless Steels by FEM. Appl Therm Eng 30(16): 2448-2459. DOI: 10.1016/j.applthermaleng.2010.06.016.

[20] Huang Y-C, Su C-H, Wu S-K, Lin C (2019) A Study on the Hall–Petch Relationship and Grain Growth Kinetics in FCC-Structured High/Medium Entropy Alloys. Entropy 21(3): 297. https://doi.org/10.3390/e21030297.

[21] Moravec J, Novakova I, Sobotka J, Neumann H (2019) Huang Y-C, Su C-H, Wu S-K, Lin C (2019) Determination of Grain Growth Kinetics and Assessment of Welding Effect on Properties of S700MC Steel in the HAZ of Welded Joints. Metals 9(6): 707. https://doi.org/10.3390/met9060707.

[22] Sello M P, Stumpf W E (2011) Laves phase precipitation and its transformation kinetics in the ferritic stainless steel type AISI 441. Mater Sci Eng A 528(3): 1840-1847. https://doi.org/10.1016/j.msea.2010.09.090.